Cellular and Molecular Life Sciences (2024) 81:432
https://doi.org/10.1007/s00018-024-05464-0

ORIGINAL ARTICLE

Long noncoding RNA AK144717 exacerbates pathological cardiac hypertrophy through modulating the cellular distribution of HMGB1 and subsequent DNA damage response

Tianyu Wu[1] · Yao Lu[2] · Yue Yu[3] · Yan Hua[1] · Gaoyuan Ge[1] · Wei Zhao[1] · Kaiyan Chen[1] · Zhuen Zhong[1] · Fengxiang Zhang[1]

Received: 3 June 2024 / Revised: 9 September 2024 / Accepted: 27 September 2024

Abstract

DNA damage induced by oxidative stress during cardiac hypertrophy activates the ataxia telangiectasia mutated (ATM)-mediated DNA damage response (DDR) signaling, in turn aggravating the pathological cardiomyocyte growth. This study aims to identify the functional associations of long noncoding RNA (lncRNAs) with cardiac hypertrophy and DDR. The altered ventricular lncRNAs in the mice between sham and transverse aortic constriction (TAC) group were identified by microarray analysis, and a novel lncRNA AK144717 was found to gradually upregulate during the development of pathological cardiac hypertrophy induced by TAC surgery or angiotensin II (Ang II) stimulation. Silencing AK144717 had a similar anti-hypertrophic effect to that of ATM inhibitor KU55933 and also suppressed the activated ATM-DDR signaling induced by hypertrophic stimuli. The involvement of AK144717 in DDR and cardiac hypertrophy was closely related to its interaction with HMGB1, as silencing HMGB1 abolished the effects of AK144717 knockdown. The binding of AK144717 to HMGB1 prevented the interaction between HMGB1 and SIRT1, contributing to the increased acetylation and then cytosolic translocation of HMGB1. Overall, our study highlights the role of AK144717 in the hypertrophic response by interacting with HMGB1 and regulating DDR, hinting that AK144717 is a promising therapeutic target for pathological cardiac growth.

Keywords LncRNAs · DNA damage response · Cardiac hypertrophy · HMGB1 acetylation

Abbreviations

ATM	Ataxia telangiectasia mutated
Ang II	Angiotensin II
DDR	DNA damage response
ECG	Electrocardiograph
ECs	Endothelial cells
HDAC1	Histone deacetylase 1
HMGB1	High-mobility group box 1
MCMECs	Mouse cardiac microvascular endothelial cells
NMCFs	Neonatal mouse cardiac fibroblasts
NMCMs	Neonatal mouse cardiomyocytes
ROS	Reactive oxygen species
SIRT1	Sirtuin 1
TAC	Transverse aortic constriction

Tianyu Wu, Yao Lu and Yue Yu contributed equally to this work.

✉ Fengxiang Zhang
njzfx6@163.com

[1] Section of Pacing and Electrophysiology, Division of Cardiology, The First Affiliated Hospital of Nanjing Medical University, Guangzhou Road 300, Nanjing 210029, PR China

[2] Department of Cardiology, Xuzhou Central Hospital, The Xuzhou School of Clinical Medicine of Nanjing Medical University, No.199 Jiefang South Road, Xuzhou 221009, PR China

[3] Department of Cardiology, Nanjing University Medical School Affiliated Nanjing Drum Tower Hospital, Zhongshan Road 321, Nanjing 210029, PR China

Published online: 12 October 2024

Introduction

Maladaptive cardiac hypertrophy is the remodeling process characterized by increased cellular sizes and unaltered total cardiomyocytes [1]. Cardiac hypertrophy followed by accumulated interstitial fibrosis resulted in reduced myocardial compliance, making it to be one of the most crucial contributors to heart failure (HF) [2]. Growing bodies of evidence verify that long noncoding RNAs (lncRNAs) are the crucial participants during pathological hypertrophy [3–6]. LncRNAs are the noncoding RNA transcripts with the length over 200 nucleotides and are capable of regulating gene expressions at transcriptional or post-transcriptional levels. LncRNAs tend to locate in nucleus and apart from regulating the gene transcriptions via the cis- or trans-regulatory methods [7], nuclear lncRNAs are reported to maintain the genome stability by binding to specific proteins [8, 9]. The bindings of lncRNAs to their proteins function either as a scaffold or as a competitor to modulate the interactions of the bound proteins with other proteins.

Activated DNA damage response (DDR) was observed in both human failing hearts and transverse aortic constriction (TAC)-induced mice heart failure model [10–13]. During pathological hypertrophy, excessive reactive oxygen species (ROS) leaking from dysfunctional mitochondria diffuse to the nucleus and cause DNA oxidative damages that activate ataxia telangiectasia mutated (ATM), the primary kinase in the DDR signaling pathway. Activated ATM then phosphorylates H2AX (phosphorylated histone H2AX, γ-H2AX) and initiates the downstream DDR pathway [14]. Although the activation of ATM-DDR pathway promoted DNA repair, recent studies reported that persistent activation of ATM exerted the detrimental roles in cardiac remodeling induced by pressure overload or myocardial infarction, making ATM activation closely related to HF progression [12, 13, 15]. Therefore, inhibiting the activation of ATM-DNA damage response pathway significantly inhibited pathological cardiac remodeling [12, 16, 17]. Moreover, LncRNAs have been confirmed to regulate the process of DNA repair and DDR [18–22], but there are no studies exploring whether the modulation of lncRNAs on DDR has impacts on hypertrophic process.

High-mobility group box 1 (HMGB1), belonging to the high-mobility group gene superfamily, acts as a non-histone nuclear DNA-binding protein. The functions of HMGB1 depend on its subcellular location, as nuclear HMGB1 participates the maintenance of genomic stability and DNA repair under physiological conditions [23, 24]. When exposed to oxidative stress or pro-hypertrophic factors, HMGB1 translocates from the nucleus to the cytosol, which is closely related to increased acetylation level of HMGB1 [25, 26]. When cytosolic HMGB1 is secreted outside cells, it functions as a damage-associated molecular pattern (DAMP) to trigger inflammatory responses and in turn exacerbates cardiac hypertrophy [27–29]. Since decreased nuclear HMGB1 due to cytoplasmic translocation was observed in failed human hearts, suppressing nuclear HMGB1 export or recovering nuclear HMGB1 were proved to alleviate cardiac hypertrophy, making nuclear HMGB1 closely related to HF development [30, 31]. What's more, preserving nuclear HMGB1 amounts was also found to suppress pathological cardiac hypertrophy through inhibiting ATM-DDR signaling [17]. Sirtuin 1 (SIRT1) or histone deacetylase 1 (HDAC1) are the most well-studied deacetylases that interact with HMGB1 and promote the deacetylation of HMGB1, thus maintaining the nuclear HMGB1 [23, 32, 33]. Under pathological circumstances, HMGB1 was found to disassociate from SIRT1 or HDAC1, contributing to increased acetylation and then nuclear export of HMGB1.

In this study, we detected the lncRNA AK144717 that was mainly expressed in the nuclei of cardiomyocytes and significantly increased along with the enhanced DDR in vivo and in vitro. We found that AK144717 modulated DDR and cardiac hypertrophy mainly through its interaction with HMGB1, which obstructed the interaction between HMGB1 and SIRT1 and promoted the acetylation and cytoplasmic translocation of HMGB1. Reduced HMGB1 in the nucleus failed to maintain the chromosome stability and suppress the activation of ATM-DDR pathway, eventually aggravating the pathologic growth of cardiomyocytes. Silencing AK144717 reduced the acetylated HMGB1 and restored the nuclear HMGB1 levels, thus suppressing the DDR signaling activation and cardiac hypertrophy. The findings in our study provide important insights into the mechanisms underlying the cytosolic translocation of HMGB1 as well as targeting AK144717 as the novel treatment for pathological hypertrophy.

Methods and materials

Establishment of TAC-induced HF mouse model

C57BL/6 mice (male, weight 22–24 g; 8-week-age-old) were purchased from Animal Centre of Nanjing Medical University. Mice were then randomly divided into the sham group ($n=6$) and TAC group ($n=10$). After anaesthetizing mice with isoflurane, sternotomy was performed along sternum midline but did not exceed the level of the second rib. After carefully separating thymus above aortic arch, a 27-G needle was placed between the left common carotid artery and truncus brachiocephalicus, and then needle and the aortic arch were tightly ligated with 7–0 nylon suture.

Withdrew the needle and sutured the sternum and skin by 5–0 nylon suture. Mice in sham group underwent the same procedures as TAC group without constricting the aorta. 7 mice in the TAC group survived 6 weeks later and together with 6 mice in the sham group were sacrificed for the following analysis after the echocardiography examination.

Echocardiography

Echocardiography examination was performed 6 weeks after TAC surgery. The mice were anesthetized with 1.5% isoflurane. Left ventricular end-systolic dimension (LVDs) and left ventricular end diastolic dimension (LVDd) were measured under M-mode echocardiography using a 30-MHz probe (Vevo 3100 System, Canada). The left ventricular ejection fraction (LVEF, %) and left ventricular fractional shortening (LVFS, %) were also calculated.

Histological analysis

Heart samples were collected at 6 weeks after TAC surgery. The hearts were fixed with 4% paraformaldehyde, embedded into paraffin and then sectioned into pieces of 5 μm. Hematoxylin-eosin (G1120, Solarbio, China) and wheat germ agglutinin (WGA, W7024, Thermo Fisher, USA) staining were then performed according to the manufacturer's instructions. Images of each sample were obtained at 40×magnifications of 5 random fields and the cardiomyocyte surface areas were calculated by Image J software (NIH).

Cell culture and treatment

Primary cardiac cells were isolated from 1- to 3-day-old C57BL/6 mice. After being anesthetized with 4% isoflurane, the hearts of neonatal mice were excised, washed and minced in Hank's balanced salt solution (HBSS, H1025-500, Solarbio, China). Then cardiac tissues were incubated with trypsin (40101ES25, Yeasen, China) and collagenase II (LS004176, Worthington-biochem, USA) at 37 °C for 1 h and washed with complete Dulbecco's modified Eagle's medium (DMEM, 11965092, Gibco, USA) and centrifuged at 1000 rpm for 5 min. Resulting cells were filtered through a 40 μm-cell strainer and plated onto a 10-cm dish. Given the differential attaching time for myocytes and non-myocytes, neonatal mouse cardiac fibroblasts (NMCFs) were obtained at about 1 h incubation in the 10-cm dish and cultured with fresh complete DMEM and harvested for RNA extraction at passage 2 or 3. Neonatal mouse cardiomyocytes (NMCMs) were obtained by differential attachment for 1 h to remove NMCFs and cultured in complete DMEM at 37 °C in 5% CO_2, 21%O_2 for the following experiments. To evaluate the roles of DDR and HMGB1 during cardiac hypertrophy, Angiotensin II (Ang II, 4474-91-3, Sigma-Aldrich, USA) was applied to establish in vitro model of cardiac hypertrophy. In detail, after starvation for 12 h, NMCMs were cultured with Ang II (100 nM) for 12 h, 24 h, 36 h and 48 h and then collected for the following experiments. For NMCMs treated with ATM inhibitor, NMCMs were pretreated with KU55933 (10 μM, HY-12016, MedChemExpress, China) for 1 h before Ang II exposure. Mouse cardiac microvascular endothelial cells (MCMECs, CP-M129, Pricella, China) were cultured in the Endothelial Cell Medium (1001, Sciencell, USA) and harvested for extracting RNA at passage 2.

Small interfering RNA (siRNA) transfection

To identify the efficiency of AK144717 knockdown, NMCMs were transfected with siRNAs targeting AK144717 (si-AK144717, 40 nM) or negative control siRNAs (NC, 40 nM) via Lipofectamine 3000 (L3000015, Invitrogen, USA) according to the manufacturer's instructions. After incubation for 6 h, si-RNAs were removed and NMCMs were cultured in the fresh serum-free medium (SFM) and AK144717 expression was checked by qRT-PCR at 24 h, 36 h and 48 h after transfection. To identify the efficiency of HMGB1 knockdown, NMCMs were transfected with siRNAs targeting HMGB1 (si-HMGB1, 40 nM) or NC and qRT-PCR analysis were applied to check HMGB1 expression at 12 h, 24 h and 36 h after transfection. To evaluate the roles of AK144717 in cardiac hypertrophy, NMCMs were divided into 4 groups: NC, Ang II + NC, si-AK144717 and Ang II + si-AK144717 group. For NC or si-AK144717 group, NMCMs were treated as described above and harvested for subsequent analysis at 48 h after transfection. In Ang II + NC and Ang II + si-AK144717 group, NMCMs were first incubated with the medium containing NC or si-AK144717 for 6 h and cultured in the SFM for another 6 h, which were then stimulated with Ang II (100 nM) for 36 h. To evaluate the necessity of HMGB1, NMCMs were divided into 4 groups: Ang II + NC, Ang II + si-AK144717, Ang II + si-HMGB1 and Ang II + si-AK144717 + si-HMGB1 group. NMCMs in Ang II + NC, Ang II + si-AK144717 and Ang II + si-HMGB1 group were treated as described above. NMCMs in Ang II + si-AK144717 + si-HMGB1 (Ang II + si-AK + si-HMGB1) group were first incubated with the medium containing si-AK144717 for 6 h, then the medium containing si-HMGB1 for another 6 h, and finally stimulated with Ang II for 36 h. All siRNAs were manufactured by GenePharma Company (China). The siRNA sequences used were listed in Supplementary Table 1.

Quantitative RT-PCR (qRT-PCR)

Total RNAs were extracted from tissues or cells by Trizol (RC202-01, Vazyme, China). The nuclear and cytoplasmic RNA was isolated and extracted by the Cytoplasmic & Nuclear RNA Purification Kit (NGB-37400, Norgen Biotek, Canada). The concentration and purity of extracted RNA was examined by a spectrophotometer (NanoDrop-2000, Thermo Fisher, USA). 1000 ng RNA was reverse-transcribed to cDNA and qRT-PCR was performed on the QuantStudio 3 real-time PCR system (Thermo Fisher, USA) with the SYBR Green (11203ES50, Yeasen, China) according to the manufacturer's instructions. 18s ribosomal RNA (18s) was the reference gene for the expression of target genes. The primers used in this article are listed in Supplementary Table 1.

Western blot

Western blot was performed according to the standard protocol as previously described [34]. The nuclear and cytoplasmic proteins were separated and extracted with the Nuclear and Cytoplasmic Extraction Kit (78835, Thermo Fisher, USA) following the manufacturer's instruction. The oxidized HMGB1 was separated by non-reducing SDS-PAGE and immunoblotted with anti-HMGB1 antibody. The antibodies included in the article were listed in Supplementary Table 2.

Enzyme linked immunosorbent assay (ELISA)

The concentrations of HMGB1 in the NMCM culture supernatants were determined with the mouse/rat HMGB1 ELISA Kit (ARG81310, Arigo, China) according to manufacturer's protocols.

Immunoprecipitation (IP) and co-immunoprecipitation (co-IP) assay

NMCMs were lysed in the lysis buffer (P0013, Beyotime, China) containing phenylmethylsulfonyl fluoride (PMSF, ST506, Beyotime, China) and deacetylase inhibitor cocktail (P1112, Beyotime, China) on ice for 30 min and centrifuged at 14,000 rpm for 10 min at 4 °C. BCA method was applied to measure the concentrations of samples. For IP assay, antibodies of HMGB1 or acetylated-lysine (Ac-lysine) or phosphorylated serine or threonine phosphor-(Ser/Thr) and IgG were added to samples overnight at 4 °C. For co-IP assay, antibodies of HMGB1, SIRT1 and appropriate Ig G were added to samples overnight at 4 °C. The mixtures were then incubated with A/G magnetic beads (88802, Thermo Fisher, USA) at room temperature for 1 h. Beads were separated with samples by the magnetic frame and washed with lysis buffer for three times. Immune complexes pulled down by magnetic beads were eluted by loading buffer containing SDS (P0015A, Beyotime, China) and resulting proteins were then checked by Western blot.

Cell immunostaining

NMCMs were fixed with 4% paraformaldehyde for 20 min and permeabilized with 0.2% Triton X-100 for 20 min. To detect cardiac hypertrophy, after blockage with 1% BSA, NMCMs were incubated with mouse anti-α-actinin (GB12555, Servicebio, China) overnight at 4 °C. The cells were washed with PBS for 5 min for three times and incubated with fluorescein isothiocyanate (FITC, 33207ES60, Yeasen, China) for 4 h at room temperature on the next day. The nucleus was stained with 4′,6-diamidino-2-phenylindole (DAPI, 40728ES03, Yeasen, China) for 3 min. Images were captured by the fluorescence microscope (Axio Vert A1, Zeiss, Germany) and analysed for the surface area of cardiomyocytes by Image J software (NIH). To detect the DDR, the DNA Damage Assay Kit by γ-H2AX Immunofluorescence (C2035S, Beyotime, China) was applied in accordance with the manufacturer's instructions and images were captured by the fluorescence microscope and analysed for the mean immunofluorescence intensity of γ-H2AX in the nucleus of cardiomyocytes by Image J software.

RNA pull-down assay

The templates for in vitro transcription were amplified by PCR and the PCR products were examined with agarose gel electrophoresis. The primers containing the T7 promoter sequence (TAATACGACTCACTATAGGG) for the amplification of AK144717 sense and antisense chains were listed in the Supplementary Table 1. The biotin-labelled AK144717 sense probes and anti-sense probes were synthesized by the RNAmax-T7 biotin-labeled transcription kit (C11002, Ribo, China). RNA pull-down assay was conducted by using Magnetic RNA-Protein Pull-Down Kit (20164, Thermo Fisher, USA) in accordance with the manufacturer's instructions. The lysates of NMCM were collected and added into tubes containing sense probe-coated beads or anti-sense probe-coated beads, which were then incubated at 4 °C for 1 h. The magnetic beads were washed and eluted to collect the protein samples which were later analysed by mass spectrometry and western blot analysis.

LC-MS/MS analysis

Protein samples pulled down by AK144717 probes were first separated by SDS-PAGE and visualized by Coomassie

blue staining, among which the interacting proteins of AK144717 antisense probes were used as a negative control. The LC-MS/MS analysis was then carried out by OE Biotech Co., Ltd (China). Finally, we screened out the substrate proteins that could bind to AK144717 according to the function and the mass of detected proteins.

RNA immunoprecipitation (RIP)

RIP was carried out by using Magna RIP RNA-binding protein immunoprecipitation kit (17–700, Millipore, USA) in accordance with the manufacturer's instructions. The NMCM lysates were collected and incubated with magnetic beads conjugated with the mouse anti-HMGB1 antibody (RIP group), or rabbit IgG (IgG group) overnight at 4 °C. The resulting RNAs were collected to synthesize cDNA and analysed by qRT-PCR.

Adeno-associated virus construction and injection

To suppress cardiac AK144717 expression in vivo, adeno-associated virus, serotype 9 (AAV9) vectors carrying shAK144717 or GFP driven by c-Tnt (troponin T) promotor (AAV9-shAK144717 or AAV9-sh-Scramble) were purchased from Genechem Company (China). To compare the therapeutic effects of silencing AK144717 and DDR inhibition, C57BL/6 mice were randomly divided into 4 groups: TAC 6w (TAC), TAC + AAV9-sh-Scramble (TAC + Scramble), TAC + AAV9-sh-Scramble + KU55933 (TAC + Scramble + KU55933) and TAC + AAV9-shAK144717 (TAC + shAK144717) group ($n = 6$ per group). The titer of AAV9 given to mice was 3×10^{11} virus genome/mouse. AAV9-shAK144717 or AAV9-sh-Scramble were injected into C57BL/6 mice through caudal veins 1 week before TAC or sham surgery. KU55933 (5 mg/kg) was intraperitoneally injected three times per week after TAC surgery.

Microarray analysis

The ventricular samples from 3 mice operated by TAC for 6 weeks and 3 mice with sham surgery were sent to Shanghai KangChen Bio-tech Company to detect the differentially expressed lncRNAs by using Arraystar mouse lncRNA microarray V4. Unpaired, two-tailed Student's t test was applied to check the differentially expressed lncRNAs between sham and TAC hearts. The differential expressed lncRNAs were identified with the fold-change > 2.0 and $P < 0.05$.

Statistical analysis

Data are expressed as mean ± SD (standard deviation). All data were analyzed by GraphPad Prism Version8 software (GraphPad Software, CA). Comparisons between two groups were analysed by unpaired, two-tailed Student's t-test and between multiple groups were analysed by one-way ANOVA with Sidak's or Tukey's test. $P < 0.05$ was considered statistically significant (* indicate $P < 0.05$, ** indicate $P < 0.01$, *** indicate $P < 0.001$, and **** indicate $P < 0.0001$), whereas NS means not significant between groups.

Results

Identification of the altered long noncoding RNAs in the mice TAC model

To investigate the roles of lncRNAs during the pathological cardiac hypertrophy, we first established the mice heart failure model by TAC surgery. Echocardiographic analysis showed the disrupted ventricular performance, including decreased LVEF and LVFS, and increased LVDs and LVDd in the mice of TAC group (Fig. 1A-C). HE staining showed the significantly enlarged cardiomyocytes, and wheat germ agglutinin (WGA) staining indicated the increased cross-sectional areas of cardiomyocytes in the TAC group (Fig. 1D-E). The increased heart weight/body weight (HW/BW) ratios were also observed in the mice of TAC group (Fig. 1F). Moreover, the hypertrophy-associated foetal genes, including atrial natriuretic peptide (ANP) and brain natriuretic peptide (BNP), were also significantly upregulated in the TAC group (Fig. 1G). Then we randomly selected three paired ventricular samples from the sham and TAC group for the microarray analysis to screen the altered genomic lncRNAs. The microarray expression profiling of lncRNAs identified 1117 upregulated and 597 downregulated lncRNAs, where the upregulated exhibited much more remarkable changes compared with the downregulated (Fig. S1A). The top 20 altered lncRNAs that all upregulated were highlighted in the volcano plot (Fig. S1B). From the top 20 altered lncRNAs, we selected the 10 lncRNAs with their detection probe signal intensities above 20 in the microarray results according to our laboratory's previous experience (Fig. 1H) (the worksheet titled "Top20 LncRNA Microarray results" in Supplementary Table S5). It should be noted that lncRNA Ndufb1-ps (ENSMUST00000221422) transcript lacks specific fragments to design qRT-PCR primers, making it almost unable to be detected. Therefore, we checked the expression of remaining 9 lncRNAs and detected 6 lncRNAs by qRT-PCR in the samples used for

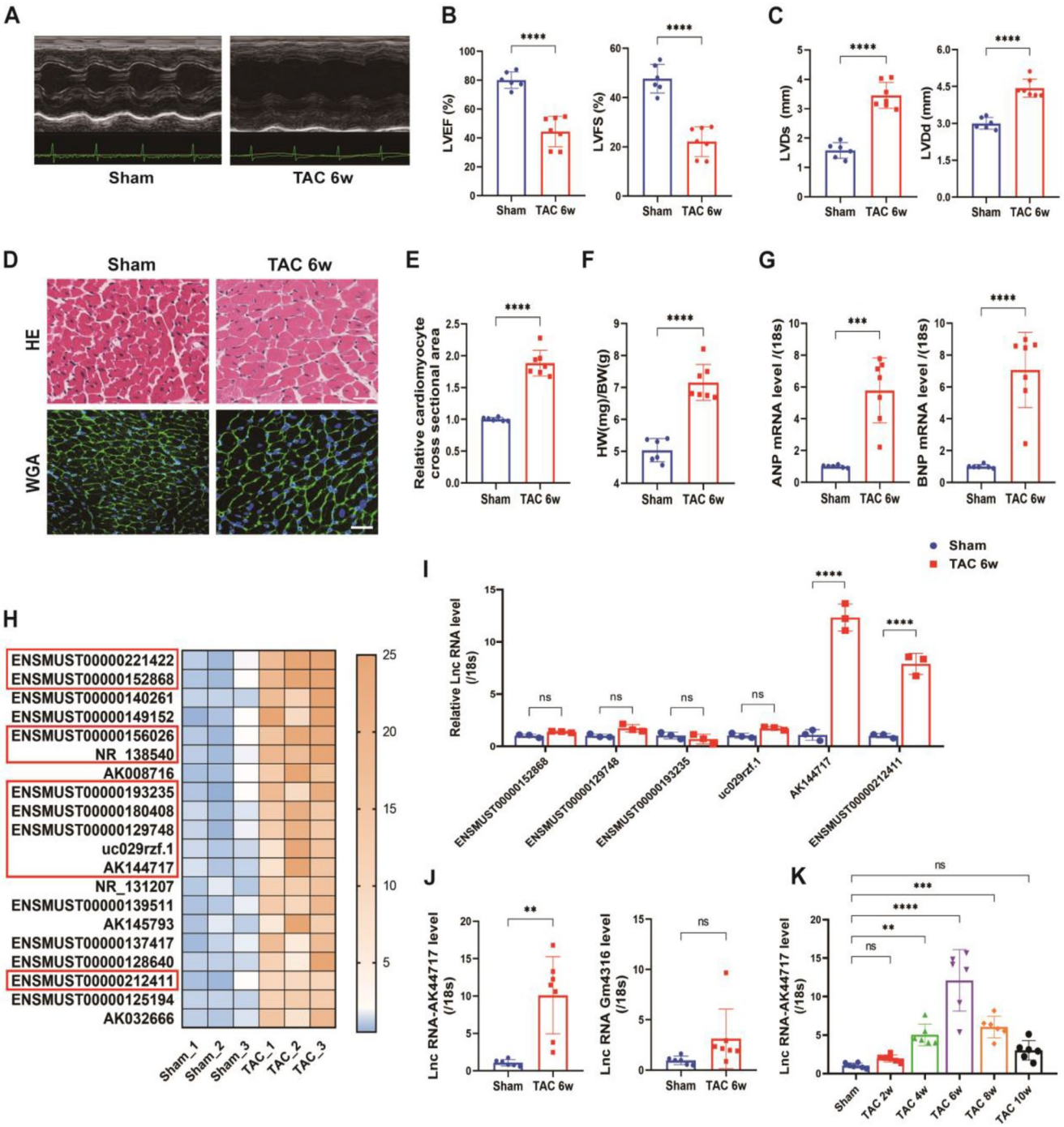

Fig. 1 Establishment of cardiac failure model and identification of altered lncRNAs. **A–C**. Echocardiography and quantitative analysis ($n=6$–7). **D–E**. Representative images of hematoxylin and eosin (H&E) staining (upper) and wheat germ agglutinin (WGA) staining ($n=6$–7). Scale bar: 100 μm. **F**. Quantitative analysis of the heart weight (HW)/body weight (BW) ratio ($n=6$–7). **G**. qPCR analysis of ANP and BNP mRNA expressions ($n=6$–7). **H**. Heat map of the top 20 altered lncRNAs in the heart. The lncRNAs with raw intensities over 20 in the microarray sequencing report are framed in red. **I**. qPCR analysis of lncRNAs in the samples applied for microarray sequencing ($n=3$). **J**. qPCR validation of LncRNA AK144717 and Gm4316 (ENSMUST00000212411) in all the mice of sham and TAC group ($n=6$–7). **K.** qPCR analysis of LncRNA AK144717 expression in the TAC models of different time ($n=6$). $^{*}P<0.05$; $^{**}P<0.01$; $^{***}P<0.001$; $^{****}P<0.0001$; NS means not significant between groups

microarray analysis, among which lncRNA AK144717 and Gm4316 (ENSMUST00000212411) showed the similar fold changes to the results of microarray analysis (Fig. 1I). However, after expanding the sample size to detect the expression of AK144717 and Gm4316, we found that the expression of Gm4316 was unstable and inconsistent with the expression in the microarray analysis, while the expression of AK144717 was still consistent with the results of the microarray (Fig. 1J). Finally, in the mice receiving TAC surgery with different time, we found the dynamic change of the expression of Gm4316 was less apparent than that in AK144717 that began to upregulate at 4 weeks after TAC surgery and reached the peak level at about 6 weeks, hinting the potential involvement of AK144717 across the process of pathological cardiac remodeling (Fig. 1K, Fig. S1C).

AK144717 knockdown suppressed TAC-induced DDR and cardiac hypertrophy

AK144717 locates at chromosome 1 with the length of more than 3000 nucleotides (Fig. S1D). Protein-Coding Potential Calculator identified AK144717 as a non-coding RNA without coding potential (Fig. S1E). We first examined the cell types that AK144717 was enriched in cardiac tissues and found it was enriched in cardiomyocytes rather than NMCFs and ECs (Fig. 2A), hinting the potential involvement of AK144717 in the pathologic growth of cardiomyocytes induced by pressure overload. lncLocator predicted that AK144717 was with high probability located in the nucleus (Fig. S1F), and we verified it and found that AK144717 primarily located in the nucleus of NMCMs (Fig. 2B). To investigate the role of AK144717 during the hypertrophic process in vivo, we silenced its expression with AAV9-shAK144717. In addition, to identify whether AK144717 participated in the vicious cycle of DNA damage response (DDR) and hypertrophic response, we compared the effects of silencing AK144717 with those of ATM inhibitor KU55933 on cardiac hypertrophy, as disrupting DDR via inhibiting ATM prevented the pathological growth of cardiomyocytes [12, 13, 17]. The procedure of in vivo functional experiments is shown in Fig. 2C. We confirmed the activation of cardiac ATM-DDR pathway 6 weeks after TAC operation, as evidenced by elevated p-ATM and γ-H2AX (Fig. 2D, E). qRT-PCR analysis indicated a about 40% decrease of cardiac AK144717 in the mice receiving AAV9-shAK144717 (Fig. 2F). Interestingly, we found that AAV9-shAK144717 and KU55933 treatment exhibited similar anti-hypertrophic effects. The upregulated ANP and BNP mRNA expressions induced by pressure overload were reversed by AAV9-shAK144717 or KU55933 (Fig. 2G, H). The attenuation of HW/BW ratios as well as the cross-sectional areas of cardiomyocyte also supported the anti-hypertrophic effects of silencing AK144717 or suppressing DDR (Fig. 2I-K). Consistently, echocardiographic analysis revealed the significant recovery of ventricular dysfunction and maladaptive remodeling driven by pressure overload in the mice receiving KU55933 or AAV9-shAK144717 (Fig. 2L-N). It is worth noting that silencing AK144717 had a slightly weaker inhibitory effect on DDR when compared with the direct ATM inhibitor (Fig. 2O). To conclude, AK144717 deficiency greatly relieved the cardiac remodeling and dysfunction in response to pressure overload, which was associated with the inhibition of ATM-DDR.

AK144717 silencing alleviated Ang II-induced hypertrophic response

To explore the mechanisms by which AK144717 regulated the hypertrophic response and its relationship with DDR, we first checked the expression of AK144717 in NMCMs stimulated by Ang II. AK144717 reached its peak level after Ang II treatment for 36 h and possessed about 4-fold increased expression (Fig. 3A). We then reduced AK144717 expression with siRNAs targeting AK144717 (si-AK144717) to explore whether it affected the hypertrophic response in vitro. After si-AK144717 transfection for 48 h, the expression of AK144717 in NMCMs decreased most significantly (Fig. 3B). The increased expression of AK144717 (Fig. 3C) as well as upregulated ANP and BNP mRNAs and enlarged cardiomyocytes (Fig. 3D-F) induced by Ang II were all significantly reversed by si-AK144717 treatment. Previous studies reported that DNA damage induced by ionizing radiation activated ATM signaling that later promoted the activation of extracellular regulated protein kinase1/2 (ERK1/2) and nuclear factor kappa-B (NF-κB) pathways, while KU55933 abolished the activated ERK1/2 and NF-κB [35–37]. Consistent to previous studies [38–42], we found the activated ERK1/2 and NF-κB pathways under Ang II exposure and silencing AK144717 significantly attenuated the upregulation of p-ERK1/2 and p-NF-κB (Fig. 3G, H). Results above indicated that AK144717 silence also alleviated the hypertrophic growth of cardiomyocytes in vitro.

AK144717 knockdown attenuated Ang II-induced DNA damage response

Activated ATM and ensuing γ-H2AX induced by Ang II stimulation were found to be reversed by AK144717 knockdown (Fig. 4A-C). In the meanwhile, silencing AK144717 had no effects on the ATM-DDR signaling under normal circumstances. We then compared the effects of KU55933 with those of AK144717 on cardiac hypertrophy in vitro. The inhibitory effect of KU55933 on Ang II-increased γ-H2AX

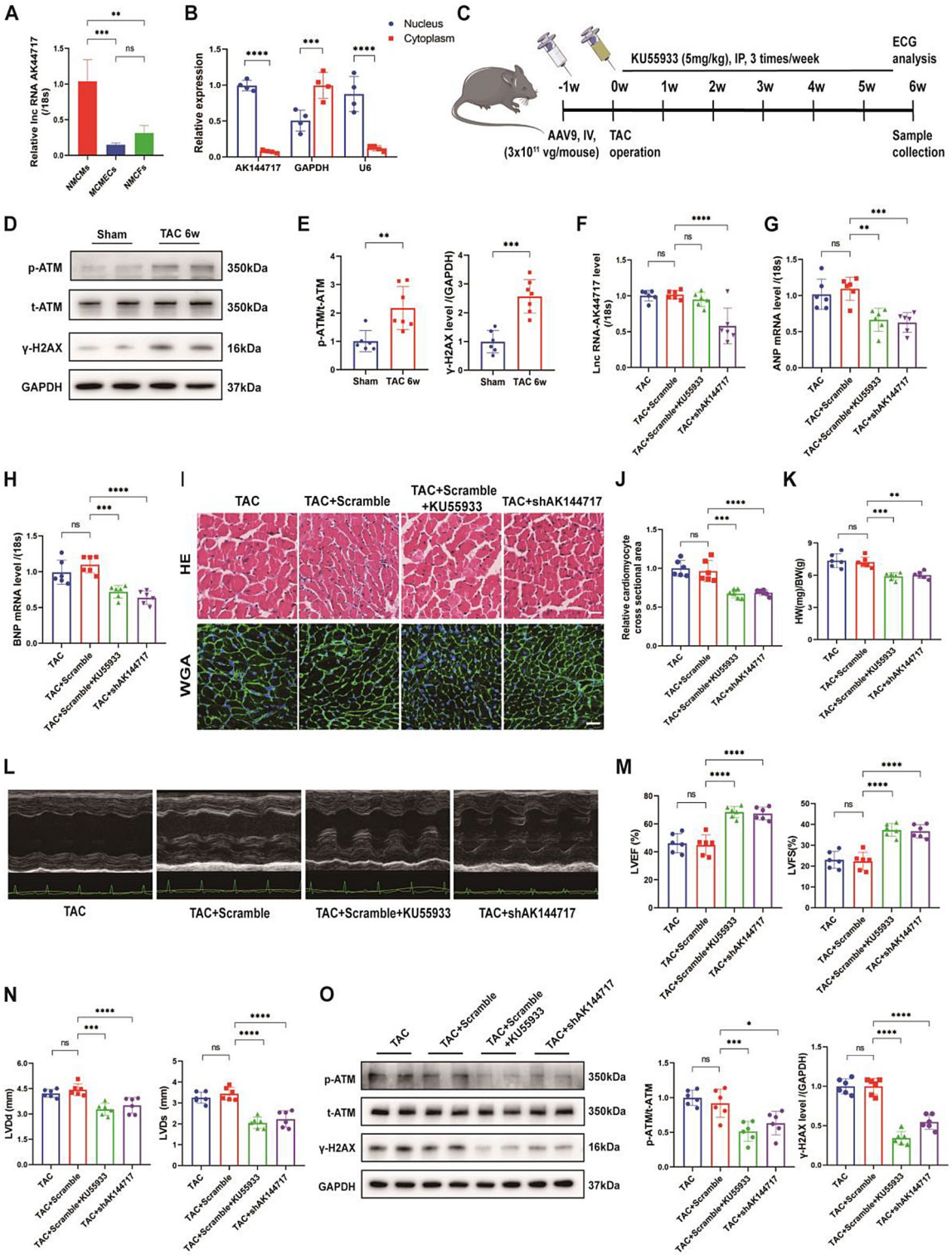

Fig. 2 AK144717 knockdown suppressed the cardiac remodeling in vivo. **A**. qPCR analysis of AK144717 expression in NMCMs, MCMECs and NMCFs ($n=3$). **B**. qPCR analysis of AK144717 expressions in the nucleus and cytoplasm of NMCMs. GAPDH and U6 were used as the cytoplasmic or the nuclear marker respectively ($n=4$). **C**. The flowchart of in vivo experiment. **D–E**. Western blot analysis of phospho-ataxia telangiectasia mutated (Ser1981) (p-ATM)/total ATM (t-ATM) and phosphorylated histone H2AX (Ser139) (γ-H2AX) ($n=6$–7). **F–H**. Quantitative analysis of AK144717, ANP and BNP mRNAs ($n=6$). **I–J**. Representative images of H&E staining (upper) and WGA staining ($n=6$). Scale bar: 100 μm. **K**. Quantitative analysis of HW/BW ratio ($n=6$). **L–N.** Echocardiography and quantitative analysis ($n=6$). **O.** Western blot analysis of p-/t-ATM, γ-H2AX ($n=6$). $^{*}P<0.05$; $^{**}P<0.01$; $^{***}P<0.001$; $^{****}P<0.0001$; NS means not significant between groups

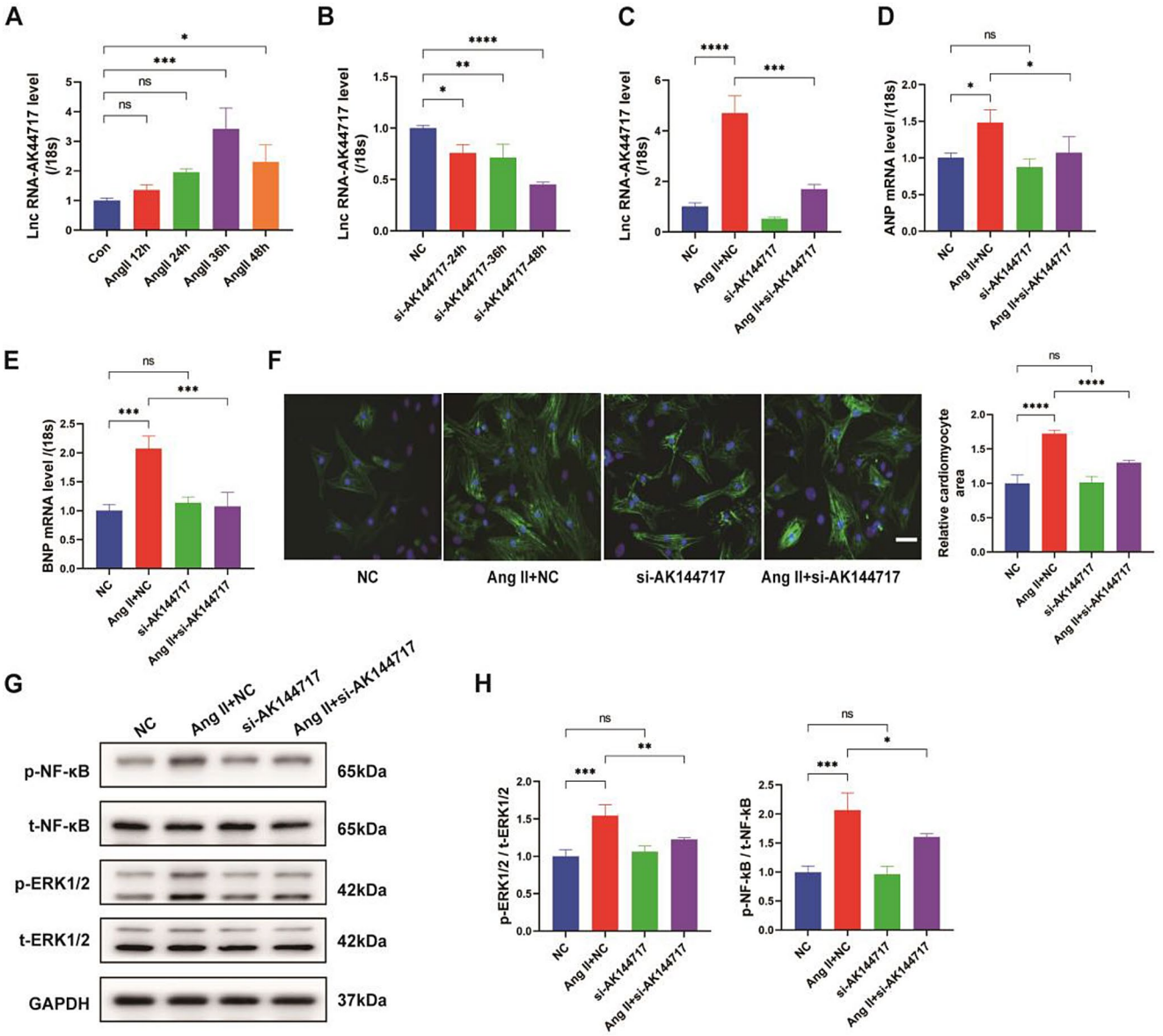

Fig. 3 AK144717 knockdown alleviated the cardiac hypertrophic response in vitro. **A**. qPCR analysis of AK144717 expression in NMCMs treated with 100 nM Ang II for different time (12 h, 24 h, 36 h, 48 h) ($n=3$). **B**. qPCR analysis of AK144717 in NMCMs transfected with si-AK144717 for 24, 36 and 48 h ($n=3$). **C–E**. qPCR analysis of AK144717, ANP and BNP mRNAs in the NMCMs treated with Ang II or si-AK144717 ($n=3$). **F**. Representative images of immunostaining (green for α-actinin, blue for DAPI) and quantitative analysis ($n=4$). Scale bar: 150 μm. **G–H**. Western blot analysis of p-/t-ERK1/2, p-/t-NF-κB ($n=3$). $^{*}P<0.05$; $^{**}P<0.01$; $^{***}P<0.001$; $^{****}P<0.0001$; NS means not significant between groups

was stronger than that of silencing AK144717 (Fig. 4D). We found that KU55933 had no effects on the AK144717 expression (Fig. 4E), but abolished the upregulated ANP and BNP and hypertrophic growth of cardiomyocytes (Fig. 4F-H), which shared the similar effects to AK144717 knockdown under Ang II stimulation. Consistently, KU55933 also alleviated the increased p-ERK and p-NF-κB (Fig. 4I). These results suggested that direct inhibition of ATM was effective in preventing myocardial hypertrophy, and AK144717 regulated the hypertrophic response at least partially through its the suppression of ATM-DDR pathway.

The inhibitory effects of AK144717 knockdown on DDR and hypertrophy were related to its interaction with HMGB1

As many nuclear lncRNAs carry out their functions by interacting with specific proteins, we proceeded to identify the proteins interacting with AK144717 that were related

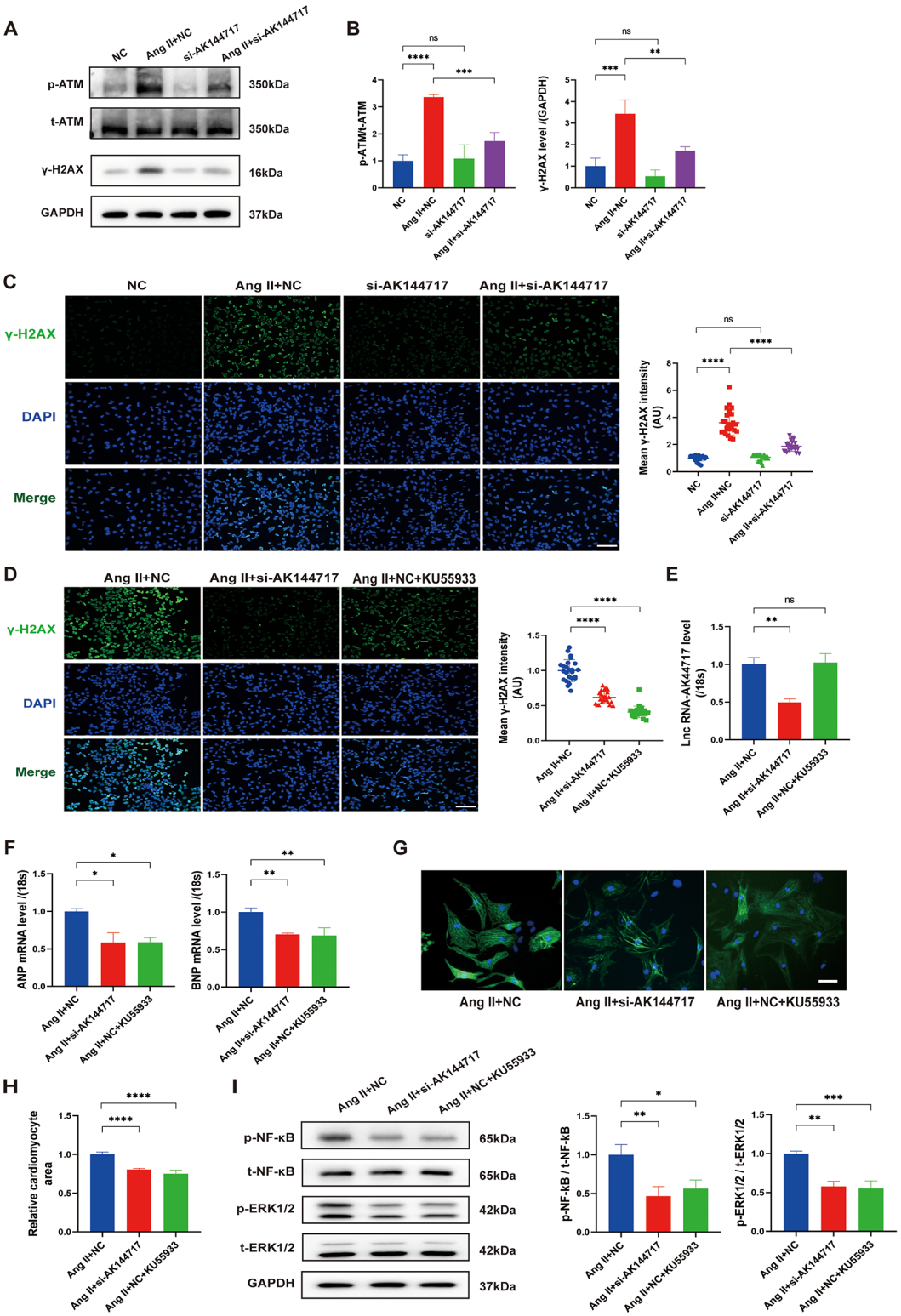

Fig. 4 AK144717 knockdown attenuated the Ang II-induced DNA damage response. **A–B**. Western blot analysis of p-/t-ATM, γ-H2AX in NMCMs treated with Ang II or si-AK144717 ($n=3$). **C–D**. Representative images of immunostaining (green for γ-H2AX, blue for DAPI) and quantification of the nuclear γ-H2AX levels in NMCMs ($n=3$). Scale bar: 500 μm; **E–F**. qPCR analysis of AK144717, ANP and BNP expression in NMCMs ($n=3$). **G–H**. Representative images of immunostaining (green for α-actinin, blue for DAPI) and quantitative analysis ($n=4$). Scale bar: 150 μm. **I.** Western blot analysis of p-ERK1/2, t-ERK1/2, p-NF-κB and t-NF-κB ($n=3$). *$P<0.05$; **$P<0.01$; ***$P<0.001$; ****$P<0.0001$; NS means not significant between groups

to its function. Coomassie blue staining of the SDS-PAGE gel showing the separated proteins pulled down by biotin-labeled AK144717 probes indicated a clear band just above the 25 kDa (Fig. 5A), which was then subjected to mass spectrometry analysis. LC-MS/MS identified 30 unique proteins were specifically enriched by AK144717 RNA instead of AK144717 antisense transcript, among which we selected 6 proteins with molecular weight near 25 kDa (Supplementary Table 3). We assessed the target proteins related to DDR and cardiac hypertrophy and thus chose HMGB1 as the target, which was also predicted to interact with AK144717 by online tool RNA-Protein Interaction Prediction (RPISeq) (Fig. S2A). Western blot analysis of the samples pulled down by AK144717 probes identified the HMGB1 as the specific protein binding to AK144717, whereas RNA immunoprecipitation (RIP) along with qRT-PCR analysis showed the enrichment of AK144717 in the samples precipitated by HMGB1 antibody rather than IgG samples (Fig. 5B, C). Online tool catRAPID further provided the interaction matrix between AK144717 and HMGB1, which exhibited the RNA and protein regions predicted to interact (Fig. 5D). To assess the necessity of HMGB1 for AK144717, we first excluded the possibility that the interaction between AK144717 and HMGB1 affected HMGB1 expression under Ang II stimulation (Fig. S2B). siRNAs targeting HMGB1 were applied to silence its expression and we found that HMGB1 significantly downregulated at 24 h to 36 h after transfection (Fig. 5E, F). Without affecting HMGB1 expression, silencing AK144717 failed to alleviate the hypertrophic responses when HMGB1 was knocked down as evidenced by the increased ANP and BNP mRNA levels (Fig. 5G, H), pathologic growth of myocytes (Fig. 5I) and activated ERK-NF-κB pathways (Fig. 5J-K). Besides, results above also indicated that silencing HMGB1 alone further exacerbated Ang II-induced hypertrophy. Moreover, silencing HMGB1 not only exacerbated Ang II-induced DDR activation, but also significantly abolished the inhibition of DDR activation generated by AK144717 knockdown (Fig. 5L-Q). Taken together, the results above suggest that the regulation of hypertrophic response by AK144717 is closely related to its interaction with HMGB1.

The interaction between AK144717 and HMGB1 modulated the acetylation and translocation of HMGB1

As elevated p-ATM and decreased nuclear HMGB1 were found in the falling human hearts [17, 30], we then investigated whether Ang II or si-AK144717 treatment affected the intracellular distribution of HMGB1. We confirmed the translocation of HMGB1 in vivo, where nuclear HMGB1 significantly reduced and cytosolic HMGB1 increased (Fig. 6A, B). Furthermore, in vitro results indicated that the cytosolic translocation of HMGB1 increased along with prolonged Ang II exposure and peaked at 36 h (Fig. 6C, D), when AK144717 also reached its maximum expression level induced by Ang II. Intriguingly, we observed that AK144717 silence greatly reduced Ang II-induced cytoplasmic relocation of HMGB1 (Fig. 6E, F). Since cytoplasmic HMGB1 would be excreted outside cells, we detected its protein amounts in cell supernatants by ELISA kit, and found that Ang II exposure obviously increased the extracellular level of HMGB1 that was significantly reversed by silencing AK144717 (Fig. 6G). In vivo results also showed that the mice treated with AAV9-shAK144717 abolished the TAC-induced translocation of HMGB1 (Fig. 6H, I). We next tried to identify the mechanisms by which AK144717 regulated the redistribution of HMGB1 under Ang II stimulation. Increased acetylation and then cytosolic translocation of HMGB1 were observed in the cardiomyocytes treated with Ang II [30, 43]. Consistently, we found that Ang II significantly increased the acetylated levels of HMGB1 whereas AK144717 knockdown reversed the enhanced HMGB1 acetylation (Fig. 6J, K), suggesting the involvement of AK144717-HMGB1 interaction in Ang II-induced acetylation and cytosolic translocation of HMGB1. Decreasing HMGB1 acetylation has been confirmed to promote its nuclear retention, and HDAC1 and SIRT1, the most studied deacetylases modifying HMGB1, are reported to physically interact with HMGB1 and deacetylate HMGB1 lysine to modulate its distribution [18, 32, 33, 44, 45]. We explored whether AK144717 affected the interaction of HMGB1 with HDAC1 or SIRT1. Ang II treatment or AK144717 silencing did not alter the protein levels of HDAC1 or SIRT1 (Fig. S2C), excluding the possibilities of AK144717 in modulating their expressions. co-IP analysis indicated that Ang II reduced the interaction between SIRT1 and HMGB1, while knockdown of AK144717 significantly reversed this reduced interaction (Fig. 6L, Fig. S2D). However, the interaction of HMGB1 to HDAC1 was not affected by either Ang II or si-AK144717 (Fig. S2E). Above results illustrated that Ang II increased the AK144717 level and thus promoted the binding of AK144717 to HMGB1, which suppressed the interaction between HMGB1 and SIRT1 and promoted translocation of HMGB1.

Discussion

Herein, we introduced a novel cardiac lncRNA AK144717 that progressively increased in cardiomyocytes undergoing sustained pressure overload. We found that silencing AK144717 not only had the similar anti-hypertrophy effect to that of DDR inhibitor KU55933, but also was

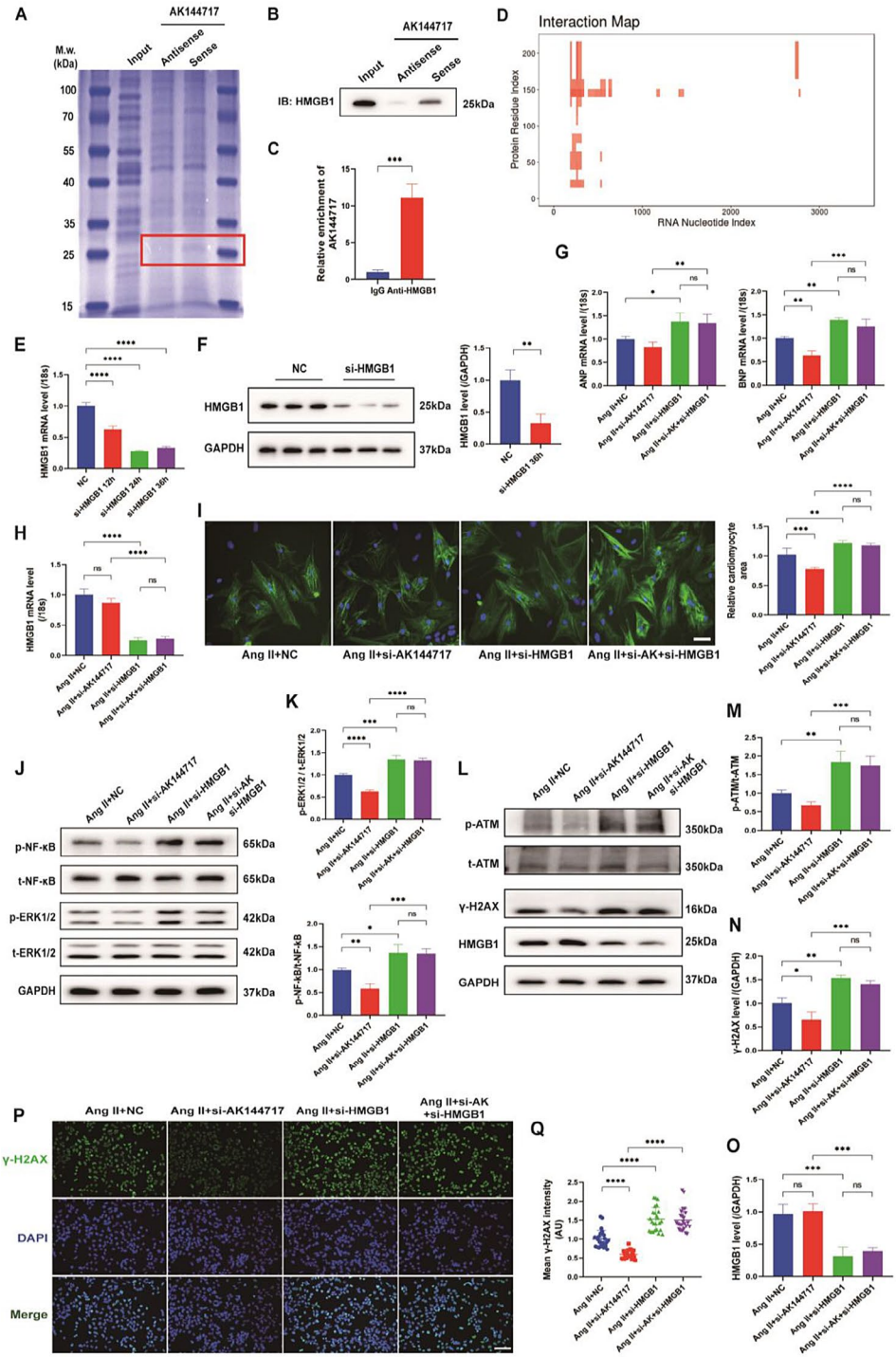

Fig. 5 AK144717 knockdown alleviated Ang II-induced DDR and hypertrophy by interacting with HMGB1. **A.** Coomassie blue staining indicated a clear protein band just above 25 kDa in the samples pulled down by the sense AK144717 probe in NMCMs. **B–C**. RNA pull down and RIP were combined to confirm the interaction between AK144717 and HMGB1 (for RIP analysis $n=3$). Anti-sense AK144717 RNA and IgG were used as the negative control respectively. **D**. The interaction matrix between AK144717 (x-axis) and HMGB1 (y-axis) was predicted by catRAPID. Red represents the interaction score. **E–F**. qPCR and Western blot analysis of HMGB1 in NMCMs transfected with siHMGB1 ($n=3$). **G–H**. qPCR analysis of HMGB1, ANP and BNP mRNAs in NMCMs treated with Ang II, si-AK144717 or si-HMGB1 ($n=3$). **I.** Representative images of immunostaining (green for α-actinin, blue for DAPI) and quantitative analysis ($n=4$). Scale bar: 150 μm. **J–O**. Western blot analysis of p-/t-ERK1/2, p-/t-NF-κB, p-/t-ATM, γ-H2AX and HMGB1 ($n=3$). **P–Q.** Representative images of immunostaining (green for γ-H2AX, blue for DAPI) and quantitative analysis. Scale bar: 300 μm. $^{*}P<0.05$; $^{**}P<0.01$; $^{***}P<0.001$; $^{****}P<0.0001$; NS means not significant between groups

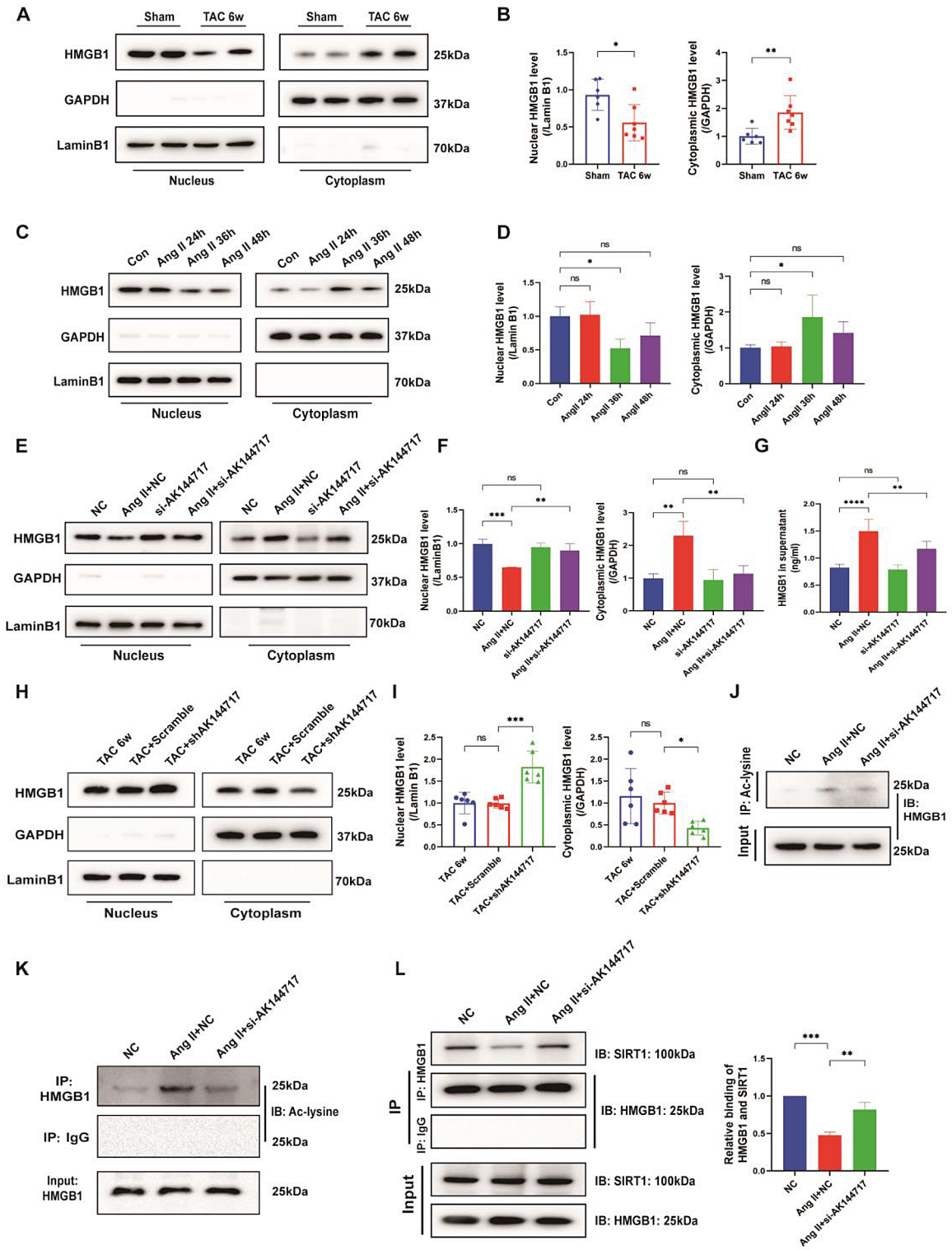

Fig. 6 AK144717 knockdown inhibited the acetylation and translocation of HMGB1 induced by Ang II. **A–B**. Western blot analysis of nuclear and cytoplasmic HMGB1 in the sham and TAC group ($n=6$–7). GAPDH and laminB1 were used as the internal control of the cytoplasmic and nuclear proteins respectively. **C–D**. Western blot analysis of nuclear and cytoplasmic HMGB1 in the NMCMs treated with Ang II for different time points (24 h, 36 h, 48 h) ($n=3$). **E–F**. Western blot analysis of nuclear and cytoplasmic HMGB1 in the NMCMs treated with Ang II or si-AK144717 ($n=3$). **G**. HMGB1 in the NMCM culture supernatants were measured by the mouse/rat HMGB1 ELISA kit ($n=6$); **H–I**. Western blot analysis of nuclear and cytoplasmic HMGB1 in the mice receiving TAC surgery or AAV9-shAK144717 injection ($n=6$). **J–K**. IP analysis of the acetylation level of lysine in HMGB1. **L**. Co-IP analysis of the interaction between SIRT1 and HMGB1 ($n=3$). $^{*}P<0.05$; $^{**}P<0.01$; $^{***}P<0.001$; $^{****}P<0.0001$; NS means not significant between groups

able to inhibit the ATM-DDR signaling in vitro and in vivo, suggesting that the regulation of AK144717 on cardiac hypertrophy was closely related to its modulation of DDR. We subsequently proved that the modulation of DDR by AK144717 was closely related to its interaction with HMGB1. In detail, the binding of AK144717 to HMGB1 enhanced the acetylated modification of HMGB1 at least partially through reducing the interaction between HMGB1 and SIRT1. Increased HMGB1 acetylation drove its continuing export from the nucleus and made it unable to maintain chromosome stability, whereas AK144717 knockdown recovered the nuclear HMGB1 level and inhibited persistent DDR activation, suggesting AK144717 may serve as a therapeutic target during the pathologic progression of cardiac hypertrophy into failure.

AK144717 began to upregulate at 4 weeks post-TAC surgery and peaked at 6 weeks post-TAC surgery when the transition from adaptative hypertrophy to heart failure with reduced ejection fraction occurred, hinting the crucial role of AK144717 in adverse cardiac remodeling during mechanic stress. We indeed found that reducing AK144717 expression attenuated pathological hypertrophy and ventricular dysfunction induced by pressure overload. Excessive DNA damage along with increased phosphorylation of ATM and subsequent DDR activation were observed in human end-stage cardiomyopathy [46]. Moreover, accumulating evidence indicated that the activation of ATM, the primary regulator of DDR, was the crucial participant during TAC-induced cardiac hypertrophy and ensuing heart failure, and suppressing ATM function or expression thus exhibited the protective effects [11–13]. Based on the previous studies illustrating the involvement of lncRNAs in DNA repair and DDR [18–22], we compared the effects of AK144717 knockdown and KU55933 on cardiac hypertrophy in vivo and in vitro respectively, and found that they shared the similar anti-hypertrophy effects. What's more, AK144717 knockdown also suppressed the ATM-DDR pathway, although its inhibitory effects were weaker than KU55933.

Given that lncRNAs usually exert their functions through binding to specific proteins, we thereafter identified the proteins interacting with AK144717 by LC-MS/MS analysis. Among the potential proteins detected, we chose the protein HMGB1 as the target of AK144717, as HMGB1 was reported to modulate both cardiac hypertrophy and DDR [17, 19, 30, 31]. RIP and western blot analysis of the samples pulled down by AK144717-sense probe further confirmed their interaction. We then identified the necessity of the interaction between HMGB1 and AK144717, which was evidenced by HMGB1 silence greatly abolished the therapeutic effects of silencing AK144717 against cardiac hypertrophy and DDR. After excluding the effects of either Ang II treatment or silencing AK144717 on HMGB1 expression, we found that their interactions regulated the intracellular distribution of HMGB1. Since ATM was demonstrated to be the downstream effector of nuclear HMGB1, diminished nuclear HMGB1 due to cytoplasmic translocation weakened its inhibitory effects on ATM and contributed to persistent activation of ATM-DDR signaling and then hypertrophic response [17]. Besides, HMGB1 in the cytoplasm would be secreted outside cells and further exacerbated cardiac hypertrophy [47]. In this article, we proved that diminishing the upregulated AK144717 driven by Ang II greatly attenuated the ensuing cytosolic translocation of HMGB1, indicating that AK144717 was the crucial participant during the HMGB1 redistribution under hypertrophic stimuli.

As deacetylated modification was the crucial regulator of HMGB1 distribution during cellular injury [48], cytoplasmic translocation of HMGB1 during cardiac remodeling was found to be highly related to its increased acetylation levels [25]. Increased total lysine acetylation levels of HMGB1 under Ang II exposure was confirmed by us and silencing AK144717 significantly reversed the enhanced HMGB1 acetylation, suggesting that AK144717 regulated HMGB1 redistribution through modulating its acetylation modification. Histone deacetylases (HDACs) are the vital modulators to deacetylate HMGB1 [23], among which HDAC1 and SIRT1 are the most studied deacetylases related to the deacetylation and translocation of HMGB1. For example, Ang II promoted the disassociation of HMGB1 from SIRT1 and resulted in the increased acetylation and release of HMGB1 from macrophages [43]. We subsequently examined whether AK144717 affected the binding of HMGB1 to HDAC1 or SIRT1, as they both have been reported to interact with HMGB1 to maintain its deacetylation. We found that Ang II weakened HMGB1's interaction with SIRT1 rather than HDAC1, and reducing AK144717 expression significantly restored the interaction between HMGB1 and SIRT1. Furthermore, catRAPID predicted the domains of HMGB1 with high interaction propensity with AK144717, among which the region 140–191 and 40–91 contained the four lysine residues of HMGB1 (Lys55, Lys88, Lys90, and Lys177) that could be deacetylated by SIRT1 (Supplementary Table 4) [48]. Among four lysine residues, Lys177 located at the nuclear localization signals (NLS) domain of HMGB1, acetylation of which was directly related to the nuclear export of HMGB1. Acetylation of the remaining three lysine residues may transform HMGB1 into a pro-damage molecule, suggesting that the association between HMGB1 and AK144717 not only affected the deacetylation of HMGB1 by SIRT1, but might alter the modulatory roles of HMGB1 in cellular response to damage. As the modification sites of phosphorylation and oxidation in HMGB1 sequence are overlapped with the domains of HMGB1 with high interaction propensity with AK144717, we also

detected the potential regulatory effects and then ruled out the possibilities that si-AK144717 treatment affected the two modifications (Fig. S2F-G).

In the end, we would discuss the limitations in this article. First of all, the confirmation of the necessity of HMGB1 might be controversial. Since AK144717 affected the distribution of HMGB1 and there is no direct inhibitor of HMGB1 nucleocytoplasmic translocation, the existing HMGB1 inhibitors, such as resveratrol [49], KPT330 [50] and inflachromene [51], also have other targets and effects, making it hard to evaluate the direct effects of inhibiting its translocation. Moreover, inhibitors targeting HMGB1 function like HMGB1-A box (Box A) tended to suppress the pro-inflammatory activities of extracellular HMGB1 [52]. Therefore, we applied siRNAs to reduce nuclear HMGB1 levels and found that silencing HMGB1 greatly abolished the anti-hypertrophic effect of AK144717 knockdown. On one hand, the anti-hypertrophic effect of AK144717 knockdown abolished by silencing HMGB1 might be due to that silencing HMGB1 itself exacerbated Ang II-induced hypertrophic response, which meant that silencing AK144717 still had the anti-hypertrophic function but in the meanwhile might be masked by the exacerbated hypertrophic response due to HMGB1 silence. On the other hand, although silencing AK144717 failed to alleviate the hypertrophic response exacerbated by HMGB1 knockdown, we could still conclude that the existence of certain amounts of nuclear HMGB1 was necessary for AK144717 to function. We could not deny that AK144717 might regulate DDR and cardiac hypertrophy even in the absence of HMGB1, but it is apparently not the major way, the function of which depends on the existence of HMGB1 instead. Second, given that AK144717 has a length over 3000 nucleotides, we next will identify the fragments of AK144717 that are responsible for the interaction with HMGB1, which would deepen us acknowledgement of the mechanisms underlying the cytosolic translocation of HMGB1. It seems that the potential clinical applications of lncRNAs are inevitable to be restricted by the poorer conservations of lncRNAs than mRNA across human beings and mice [53, 54]. Conversely, the concept of "functional conservation" was introduced and supported by accumulative evidence, which illustrated lncRNAs may be functionally conserved even though they had very short or no sequence similarities [55–58]. Since this concept highlights that the judgement of the functional significance of lncRNAs should not be limited to the conservation at the sequence level, it inspires us to focus on the process with potential conservation, such as the production of lncRNA, and also judge their functional significance by the rigorous functional experiments in each species. Third, although recovering nuclear HMGB1 was helpful to maintain chromatin stability and genomic homeostasis, the exact mechanism by which nuclear HMGB1 inhibited ATM activation largely remained unknown. Besides, although AK144717 was found to be enriched in cardiomyocytes, it cannot deny that AK144717 in NMCFs or ECs might also participate the transition from hypertrophy to heart failure. Fourth, this study utilized AAV9 virus to knock down AK144717 rather than using mouse knockout or conditional knockout models, which diminishes the strength of the evidence regarding lncRNA144717's impacts on pathological cardiac hypertrophy. Finally, we only checked whether SIRT1 or HDAC1, the two deacetylases reported to be capable of interacting with HMGB1, were affected by Ang II or si-AK144717. It was not clear whether other deacetylases were also affected, which would also be the focus of our future work.

Conclusion

To conclude, we identified a novel lncRNA AK144717 that gradually upregulated during TAC-induced heart failure progression. We found that AK144717 bound to HMGB1 and promoted its cytoplasmic translocation under Ang II stimulation, which could be attributed to the decreased interaction between HMGB1 and SIRT1 and then increased acetylation of HMGB1. What's more, when AK144717 was knocked down, the decreased interaction between HMGB1 and SIRT1 as well as the increased acetylation of HMGB1 were significantly reversed, contributing to the recovery of nuclear HMGB1 and thus attenuating the hypertrophic stimuli-induced sustained activation of ATM-DDR pathway.

Supplementary Information The online version contains supplementary material available at https://doi.org/10.1007/s00018-024-05464-0.

Acknowledgements Not applicable.

Author contributions Conceptualization, Tianyu Wu and Yao Lu; methodology, Tianyu Wu and Yue Yu; software, Wei Zhao; data curation, Kaiyan Chen and Zhuen Zhong; writing—original draft preparation, Tianyu Wu, Yao Lu and Yan Hua; writing—review and editing, Yao Lu and Fengxiang Zhang; visualization, Wei Zhao, Gaoyuan Ge; supervision, Gaoyuan Ge and Fengxiang Zhang; project administration, Fengxiang Zhang; funding acquisition, Fengxiang Zhang All authors read and approved the final manuscript.

Funding This research was funded by the National Natural Science Foundation of China (Grant No. 82370333, 82170321 and 81871113), the Jiangsu Provincial Natural Science Fund (BK20201489), the 333 project of Jiangsu Province (2022-2-408).

Data availability The datasets generated during and analysed during the current study are not publicly available due to the ongoing further research but are available from the corresponding author on reasonable request.

Declarations

Ethical approval All the protocols of animal experiments were approved by the Ethics Committee of Nanjing Medical University (IACUC-2205047) and in accordance with the Guide for the Care and Use of Laboratory Animals announced by the U. S. National Institutes of Health (NIH).

Consent for publication Not applicable.

Competing interests The authors have declared that no competing interest exists.

References

1. Nakamura M, Sadoshima J (2018) Mechanisms of physiological and pathological cardiac hypertrophy. Nat Rev Cardiol 15:387–407. https://doi.org/10.1038/s41569-018-0007-y
2. Savarese G, Lund LH (2017) Global Public Health Burden of Heart Failure. Card Fail Rev 3:7–11. https://doi.org/10.15420/cfr.2016:25
3. Wang YW et al (2022) HIF-1alpha-regulated lncRNA-TUG1 promotes mitochondrial dysfunction and pyroptosis by directly binding to FUS in myocardial infarction. Cell Death Discov 8:178. https://doi.org/10.1038/s41420-022-00969-8
4. Sato M et al (2021) The lncRNA Caren antagonizes heart failure by inactivating DNA damage response and activating mitochondrial biogenesis. Nat Commun 12:2529. https://doi.org/10.1038/s41467-021-22735-7
5. Li H et al (2022) lncExACT1 and DCHS2 regulate physiological and pathological Cardiac Growth. Circulation 145:1218–1233. https://doi.org/10.1161/CIRCULATIONAHA.121.056850
6. Hoepfner J et al (2022) The long non-coding RNA NRON promotes the development of cardiac hypertrophy in the murine heart. Mol Ther 30:1265–1274. https://doi.org/10.1016/j.ymthe.2021.11.018
7. Beucher A et al (2022) The HASTER lncRNA promoter is a cis-acting transcriptional stabilizer of HNF1A. Nat Cell Biol 24:1528–1540. https://doi.org/10.1038/s41556-022-00996-8
8. Wu Y et al (2022) MNX1-AS1, a c-Myc induced lncRNA, promotes the Warburg effect by regulating PKM2 nuclear translocation. J Exp Clin Cancer Res 41:337. https://doi.org/10.1186/s13046-022-02547-3
9. Chen R et al (2017) Quantitative proteomics reveals that long non-coding RNA MALAT1 interacts with DBC1 to regulate p53 acetylation. Nucleic Acids Res 45:9947–9959. https://doi.org/10.1093/nar/gkx600
10. Suzuki S et al (2011) 8-Hydroxy-2'-deoxyguanosine is a prognostic mediator for cardiac event. Eur J Clin Invest 41:759–766. https://doi.org/10.1111/j.1365-2362.2010.02465.x
11. Zhao B, Bouchareb R, Lebeche D (2022) Resistin deletion protects against heart failure injury by targeting DNA damage response. Cardiovasc Res 118:1947–1963. https://doi.org/10.1093/cvr/cvab234
12. Nakada Y et al (2019) DNA damage response mediates pressure overload-Induced Cardiomyocyte Hypertrophy. Circulation 139:1237–1239. https://doi.org/10.1161/CIRCULATIONAHA.118.034822
13. Higo T et al (2017) DNA single-strand break-induced DNA damage response causes heart failure. Nat Commun 8:15104. https://doi.org/10.1038/ncomms15104
14. Shiloh Y, Ziv Y (2013) The ATM protein kinase: regulating the cellular response to genotoxic stress, and more. Nat Rev Mol Cell Biol 14:197–210. https://doi.org/10.1038/nrm3546
15. Daniel LL et al (2014) Deficiency of ataxia telangiectasia mutated kinase delays inflammatory response in the heart following myocardial infarction. J Am Heart Assoc 3:e001286. https://doi.org/10.1161/JAHA.114.001286
16. Khan K, Makhoul G, Yu B, Schwertani A, Cecere R (2019) The cytoprotective impact of yes-associated protein 1 after ischemia-reperfusion injury in AC16 human cardiomyocytes. Exp Biol Med (Maywood) 244:802–812. https://doi.org/10.1177/1535370219851243
17. Takahashi T et al (2019) Cardiac Nuclear High-Mobility Group Box 1 ameliorates pathological cardiac hypertrophy by inhibiting DNA damage response. JACC Basic Transl Sci 4:234–247. https://doi.org/10.1016/j.jacbts.2018.11.011
18. Zhang B, Thorne RF, Zhang P, Wu M, Liu L (2022) Vanguard is a glucose deprivation-responsive long non-coding RNA essential for chromatin Remodeling-Reliant DNA repair. Adv Sci (Weinh) 9:e2201210. https://doi.org/10.1002/advs.202201210
19. Lou MM et al (2021) Long noncoding RNA BS-DRL1 modulates the DNA damage response and genome stability by interacting with HMGB1 in neurons. Nat Commun 12:4075. https://doi.org/10.1038/s41467-021-24236-z
20. Yu R et al (2022) LncRNA CTBP1-DT-encoded microprotein DDUP sustains DNA damage response signalling to trigger dual DNA repair mechanisms. Nucleic Acids Res 50:8060–8079. https://doi.org/10.1093/nar/gkac611
21. La T et al (2023) LncRNA LIMp27 regulates the DNA damage response through p27 in p53-Defective Cancer cells. Adv Sci (Weinh) 10:e2204599. https://doi.org/10.1002/advs.202204599
22. Chuang TW, Su CH, Wu PY, Chang YM, Tarn WY (2023) LncRNA HOTAIRM1 functions in DNA double-strand break repair via its association with DNA repair and mRNA surveillance factors. Nucleic Acids Res. https://doi.org/10.1093/nar/gkad143
23. Bonaldi T et al (2003) Monocytic cells hyperacetylate chromatin protein HMGB1 to redirect it towards secretion. EMBO J 22:5551–5560. https://doi.org/10.1093/emboj/cdg516
24. Chen R, Kang R, Tang D (2022) The mechanism of HMGB1 secretion and release. Exp Mol Med 54:91–102. https://doi.org/10.1038/s12276-022-00736-w
25. Wang Y, Wang L, Gong Z (2019) Regulation of Acetylation in High Mobility Group protein B1 cytosol translocation. DNA Cell Biol 38:491–499. https://doi.org/10.1089/dna.2018.4592
26. Chen H, Liu J, Wang B, Li Y (2020) Protective effect of lncRNA CRNDE on myocardial cell apoptosis in heart failure by regulating HMGB1 cytoplasm translocation through PARP-1. Arch Pharm Res 43:1325–1334. https://doi.org/10.1007/s12272-020-01290-7
27. Zhang L et al (2016) Extracellular high-mobility group box 1 mediates pressure overload-induced cardiac hypertrophy and

heart failure. J Cell Mol Med 20:459–470. https://doi.org/10.1111/jcmm.12743
28. Su FF et al (2012) High-mobility group box 1 induces calcineurin-mediated cell hypertrophy in neonatal rat ventricular myocytes. *Mediators Inflamm* 805149, https://doi.org/10.1155/2012/805149 (2012)
29. Lin H et al (2016) HMGB1-RAGE Axis makes no contribution to Cardiac Remodeling Induced by pressure-overload. PLoS ONE 11:e0158514. https://doi.org/10.1371/journal.pone.0158514
30. Funayama A et al (2013) Cardiac nuclear high mobility group box 1 prevents the development of cardiac hypertrophy and heart failure. Cardiovasc Res 99:657–664. https://doi.org/10.1093/cvr/cvt128
31. Li Q et al (2019) PARP1 interacts with HMGB1 and promotes its nuclear export in pathological myocardial hypertrophy. Acta Pharmacol Sin 40:589–598. https://doi.org/10.1038/s41401-018-0044-4
32. Wei S et al (2019) SIRT1-mediated HMGB1 deacetylation suppresses sepsis-associated acute kidney injury. Am J Physiol Ren Physiol 316:F20–F31. https://doi.org/10.1152/ajprenal.00119.2018
33. Chen X et al (2018) Omega-3 polyunsaturated fatty acid attenuates the inflammatory response by modulating microglia polarization through SIRT1-mediated deacetylation of the HMGB1/NF-kappaB pathway following experimental traumatic brain injury. J Neuroinflammation 15:116. https://doi.org/10.1186/s12974-018-1151-3
34. Yu Y et al (2022) Exosomal thioredoxin-1 from hypoxic human umbilical cord mesenchymal stem cells inhibits ferroptosis in doxorubicin-induced cardiotoxicity via mTORC1 signaling. Free Radic Biol Med 193:108–121. https://doi.org/10.1016/j.freeradbiomed.2022.10.268
35. Piret B, Schoonbroodt S, Piette J (1999) The ATM protein is required for sustained activation of NF-kappaB following DNA damage. Oncogene 18:2261–2271. https://doi.org/10.1038/sj.onc.1202541
36. Golding SE et al (2007) Extracellular signal-related kinase positively regulates ataxia telangiectasia mutated, homologous recombination repair, and the DNA damage response. Cancer Res 67:1046–1053. https://doi.org/10.1158/0008-5472.CAN-06-2371
37. Ahmed KM et al (2009) Coactivation of ATM/ERK/NF-kappaB in the low-dose radiation-induced radioadaptive response in human skin keratinocytes. Free Radic Biol Med 46:1543–1550. https://doi.org/10.1016/j.freeradbiomed.2009.03.012
38. Qin J, Liu ZX (2006) FAK-related nonkinase attenuates hypertrophy induced by angiotensin-II in cultured neonatal rat cardiac myocytes. Acta Pharmacol Sin 27:1159–1164. https://doi.org/10.1111/j.1745-7254.2006.00370.x
39. Liu C et al (2010) Allicin protects against cardiac hypertrophy and fibrosis via attenuating reactive oxygen species-dependent signaling pathways. J Nutr Biochem 21:1238–1250. https://doi.org/10.1016/j.jnutbio.2009.11.001
40. Lim S et al (2018) sRAGE attenuates angiotensin II-induced cardiomyocyte hypertrophy by inhibiting RAGE-NFkappaB-NLRP3 activation. Inflamm Res 67:691–701. https://doi.org/10.1007/s00011-018-1160-9
41. Li HL et al (2005) Isorhapontigenin, a new resveratrol analog, attenuates cardiac hypertrophy via blocking signaling transduction pathways. Free Radic Biol Med 38:243–257. https://doi.org/10.1016/j.freeradbiomed.2004.10.020
42. Chen G et al (2014) Puerarin inhibits angiotensin II-induced cardiac hypertrophy via the redox-sensitive ERK1/2, p38 and NF-kappaB pathways. Acta Pharmacol Sin 35:463–475. https://doi.org/10.1038/aps.2013.185
43. Zhou S et al (2018) Angiotensin II enhances the acetylation and release of HMGB1 in RAW264.7 macrophage. Cell Biol Int 42:1160–1169. https://doi.org/10.1002/cbin.10984
44. Novelli F et al (2021) BAP1 forms a trimer with HMGB1 and HDAC1 that modulates gene x environment interaction with asbestos. Proc Natl Acad Sci U S A 118. https://doi.org/10.1073/pnas.2111946118
45. Xu W et al (2014) Novel role of resveratrol: suppression of high-mobility group protein box 1 nucleocytoplasmic translocation by the upregulation of sirtuin 1 in sepsis-induced liver injury. Shock 42:440–447. https://doi.org/10.1097/SHK.0000000000000225
46. Siggens L, Figg N, Bennett M, Foo R (2012) Nutrient deprivation regulates DNA damage repair in cardiomyocytes via loss of the base-excision repair enzyme OGG1. FASEB J 26:2117–2124. https://doi.org/10.1096/fj.11-197525
47. Wahid A, Chen W, Wang X, Tang X (2021) High-mobility group box 1 serves as an inflammation driver of cardiovascular disease. Biomed Pharmacother 139:111555. https://doi.org/10.1016/j.biopha.2021.111555
48. Rabadi MM et al (2015) High-mobility group box 1 is a novel deacetylation target of Sirtuin1. Kidney Int 87:95–108. https://doi.org/10.1038/ki.2014.217
49. Delucchi F et al (2012) Resveratrol treatment reduces cardiac progenitor cell dysfunction and prevents morpho-functional ventricular remodeling in type-1 diabetic rats. PLoS ONE 7:e39836. https://doi.org/10.1371/journal.pone.0039836
50. Wu M et al (2018) KPT-330, a potent and selective CRM1 inhibitor, exhibits anti-inflammation effects and protection against sepsis. Biochem Biophys Res Commun 503:1773–1779. https://doi.org/10.1016/j.bbrc.2018.07.112
51. Lee S et al (2014) A small molecule binding HMGB1 and HMGB2 inhibits microglia-mediated neuroinflammation. Nat Chem Biol 10:1055–1060. https://doi.org/10.1038/nchembio.1669
52. Agalave NM et al (2014) Spinal HMGB1 induces TLR4-mediated long-lasting hypersensitivity and glial activation and regulates pain-like behavior in experimental arthritis. Pain 155:1802–1813. https://doi.org/10.1016/j.pain.2014.06.007
53. Schonrock N, Harvey RP, Mattick JS (2012) Long noncoding RNAs in cardiac development and pathophysiology. Circ Res 111:1349–1362. https://doi.org/10.1161/CIRCRESAHA.112.268953
54. Devaux Y et al (2015) Long noncoding RNAs in cardiac development and ageing. Nat Rev Cardiol 12:415–425. https://doi.org/10.1038/nrcardio.2015.55
55. Diederichs S (2014) The four dimensions of noncoding RNA conservation. Trends Genet 30:121–123. https://doi.org/10.1016/j.tig.2014.01.004
56. Carlevaro-Fita J et al (2020) Cancer LncRNA Census reveals evidence for deep functional conservation of long noncoding RNAs in tumorigenesis. Commun Biol 3:56. https://doi.org/10.1038/s42003-019-0741-7
57. Kirk JM et al (2018) Functional classification of long non-coding RNAs by k-mer content. Nat Genet 50:1474–1482. https://doi.org/10.1038/s41588-018-0207-8
58. Marin-Bejar O et al (2017) The human lncRNA LINC-PINT inhibits tumor cell invasion through a highly conserved sequence element. Genome Biol 18:202. https://doi.org/10.1186/s13059-017-1331-y